Nanoscale

RSC Publishing

PAPER

View Article Online
View Journal | View Issue

Cite this: *Nanoscale*, 2013, **5**, 9875

Solution-phase synthesis of single-crystal Cu_3Si nanowire arrays on diverse substrates with dual functions as high-performance field emitters and efficient anti-reflective layers†

Fang-Wei Yuan,[a] Chiu-Yen Wang,[b] Guo-An Li,[a] Shu-Hao Chang,[a] Li-Wei Chu,[b] Lih-Juann Chen[b] and Hsing-Yu Tuan*[a]

Received 13th June 2013
Accepted 26th July 2013

DOI: 10.1039/c3nr03045h

www.rsc.org/nanoscale

There is strong and growing interest in applying metal silicide nanowires as building blocks for a new class of silicide-based applications, including spintronics, nano-scale interconnects, thermoelectronics, and anti-reflective coating materials. Solution-phase environments provide versatile materials chemistry as well as significantly lower production costs compared to gas-phase synthesis. However, solution-phase synthesis of silicide nanowires remains challenging due to the lack of fundamental understanding of silicidation reactions. In this study, single-crystalline Cu_3Si nanowire arrays were synthesized in an organic solvent. Self-catalyzed, dense single-crystalline Cu_3Si nanowire arrays were synthesized by thermal decomposition of monophenylsilane in the presence of copper films or copper substrates at 420 to 475 °C and 10.3 MPa in supercritical benzene. The solution-grown Cu_3Si nanowire arrays serve dual functions as field emitters and anti-reflective layers, which are reported on copper silicide materials for the first time. Cu_3Si nanowires exhibit superior field-emission properties, with a turn-on-voltage as low as 1.16 V μm^{-1}, an emission current density of 8 mA cm^{-2} at 4.9 V μm^{-1}, and a field enhancement factor (β) of 1500. Cu_3Si nanowire arrays appear black with optical absorption less than 5% between 400 and 800 nm with minimal reflectance, serving as highly efficient anti-reflective layers. Moreover, the Cu_3Si nanowires could be grown on either rigid or flexible substrates (PI). This study shows that solution-phase silicide reactions are adaptable for high-quality silicide nanowire growth and demonstrates their promise towards fabrication of metal silicide-based devices.

Introduction

Metal–silicon interactions and the resulting silicides play important roles in the semiconductor industry. Traditionally in electronic circuitry, metallic silicides have been widely used for Schottky diodes, metal gates, and local interconnections in complementary metal oxide-semiconductor (CMOS) devices.[1,2] In recent years, one-dimensional metal silicide nanowires have been employed as building blocks for a new class of silicide-based applications, such as field emitters, spintronics, nano-scale interconnects, and anti-reflective layers.[3–7] The major challenging issues for the controlled growth of silicide nanomaterials are their many possible phases from metal-rich to silicon-rich silicides and complex phase behaviors within a narrow composition range. The main synthetic protocols for silicide nanowire growth involve gas-phase reactions due to their well-established precursor chemistry for silicide formation and fabrication processes.[8–11] A variety of metal silicide nanowires have been achieved by either silicidation of silicon nanowires,[12–14] delivery of Si flux on metal films,[7,10,11,15] reactions of metals with silicon substrates,[16,17] or co-pyrolysis of organometallic precursors of metals and silicon *via* chemical vapor deposition (CVD) and chemical vapor transport (CVT).[18–20]

Solution-phase synthesis offers significantly lower production cost compared to gas-phase synthesis when considering relevant factors such as throughput rate, equipment price, and process cost. A solvent-based environment provides versatile materials chemistry to produce a variety of high-quality nanowires or complex structures.[21,22] However, there have been no examples of growth of silicide nanowires by solution-phase reactions. There is a lack of fundamental understanding regarding suitable Si and metal precursors to address silicidation chemistry in solution-phase reactions. In addition, the accessible temperature range for solution-phase silicidation is limited to values less than 650 °C (the decomposition temperature of organic solvents),

[a]*Department of Chemical Engineering, National Tsing Hua University, 101, Section 2, Kuang-Fu Road, Hsinchu, Taiwan 30013, Republic of China. E-mail: hytuan@che.nthu.edu.tw; Fax: +86-3-571-5408; Tel: +86-3-572-3661*

[b]*Department of Materials Science and Engineering, National Tsing Hua University, Hsinchu, Taiwan 30013, Republic of China*

† Electronic supplementary information (ESI) available: Additional SEM, TEM images, and FTIR spectrum of Cu_3Si nanowires. See DOI: 10.1039/c3nr03045h

relatively cold with respect to accessible gas-phase temperatures (>1200 °C). Moreover, in the reported literature, transition metals such as Ni, Cu, and Ti function as seeds to grow Si nanowires by solution-phase reactions containing metals and silicon precursors.[23–25] Therefore, it is essential to balance related synthetic parameters, including precursor decomposition kinetics, reaction temperatures, and synthetic modes preferable for silicide nanowire growth.

Here we report the first example of solution-phase growth of metal silicide nanowires. Single-crystalline Cu_3Si nanowire arrays with diameters ranging from 50 to 150 nm were synthesized by thermal decomposition of monophenylsilane (MPS) in the presence of copper films or copper substrates in supercritical benzene. As shown in Scheme 1, diffusion-based Si–Cu reactions initiate self-catalyzed, spontaneous growth of Cu_3Si nanowire arrays at the interface between Si flux and Cu substrates.

The obtained solution-grown Cu_3Si nanowire arrays serve dual functions. First, Cu_3Si nanowires were explored as field emitters; they displayed superior field-emission properties, with a turn-on-voltage as low as 1.16 V μm^{-1}, an emission current density of 8 mA cm^{-2} at 4.9 V μm^{-1}, and a field enhancement factor (β) of 1500, and appeared to be promising as candidates for optoelectronic devices. Second, Cu_3Si nanowire arrays were studied for their anti-reflective properties; they appeared black, showing strong optical absorption less than 5% in the wavelength range of 400 to 800 nm with minimal reflectance, serving as highly anti-reflective coating materials. Moreover, Cu_3Si nanowires can be grown on either rigid or flexible substrates, including copper foil, transparent glass, and polyimide (PI), thus providing a versatile platform for a wide range of practical uses. This study shows that the solution-phase reactions can serve as viable routes for the preparation of silicide nanowires with multifunctional properties and as an advantageous fabrication process for silicide devices.

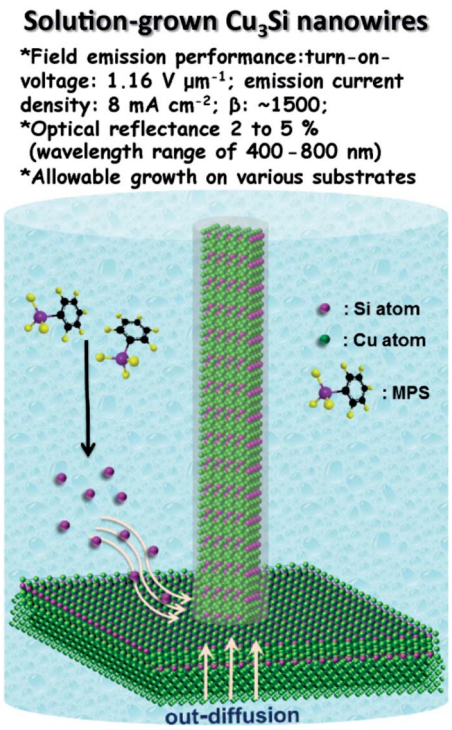

Scheme 1 Schematic diagram of solution-grown Cu_3Si nanowires on a Cu substrate. The nanowire arrays have superior field emission and antireflective properties, and can be grown on a variety of substrates.

Materials and methods

Materials

Anhydrous benzene was purchased from Sigma-Aldrich; monophenylsilane (MPS, 97%) was purchased from Gelest. All chemicals were stored in an argon-filled box and used as received. Copper substrates were purchased from the Taiwan non-ferrous-metal company. Copper foil (0.01 mm, 99.99%) was purchased from Shining Energy Co., Ltd. Polyimide (PI) tape was purchased from Grand-Hand company and the glass substrate was purchased from Tung-Kuang company in Taiwan.

Cu_3Si nanowire synthesis

Copper substrates were cleaned with acetone and toluene. Cu films were pre-deposited on glass and PI tape. Cu films with a thickness of 0.5 to 1 μm (film thickness monitor, MDC-360) were deposited using electron beam evaporation (EBS-500) in a vacuum of 5×10^{-6} torr. The deposition rate was 1.0 angstrom per s.

Growth of Cu_3Si nanowires was carried out through a semi-batch reaction in a 10 ml titanium grade reactor. The reactor containing substrates inside was first placed into an argon-filled glove box to make it free of oxygen, and then was brought out from the glove box. The reactor cell was covered with heating tape and insulated with the temperature maintained within ±1.0 °C. The inlet of the 10 ml Ti reactor cell was connected to high-pressure (1/16″ i.d.) tubing *via* a LM-6 HIP (High Pressure Equipment Co.) reducer. The inlet 1/16″ stainless steel tubing was connected to a six-way valve (valco) with a 0.5 ml injection cylinder. A high pressure liquid chromatography (HPLC) pump (Lab Alliance, series 1500) connected to the six-way valve was used to deliver the reactant solution into the reactor as well as to pressurize the reactor. The reactor pressure was monitored with a digital pressure gauge (Yan-Chang Technology). The reactant solution was prepared in the glove box. Pure MPS was diluted using anhydrous benzene at 500 mM to 1.0 M in concentration. In a typical semi-batch nanowire reaction, the reactor was heated to reaction temperature (420 to 475 °C) and pressurized to 5.5 MPa. Then a 1.0 ml reactant solution was removed from the glove box and injected into the injection loop. The reactant mixture was injected to the reactor at a flow rate of 0.5 ml min^{-1}. The HPLC pump was turned off when the system reached a final pressure of 10.3 MPa. After 5 min, the reactor was submerged in a water bath until it reached room temperature. The reacted substrates covered with Cu_3Si nanowires were removed from the reactor for further characterization.

To grow Cu_3Si films, thin film diffusion couples of Cu and Si were prepared. Cu films with a thickness of 200 to 300 nm were deposited on Si wafers by electron beam evaporation. Before loading into the evaporation chamber, Si wafers were etched in buffered HF, rinsed, and dried. Then the substrates were put into a hot-wall chemical vapor deposition (CVD) system.

Subsequently, 20 standard cubic centimeters per minute (sccm) H_2 and 180 sccm N_2 were introduced into the reactor and the pressure was evacuated to 0.5 torr. The temperature of the quartz tube was raised to 400 to 500 °C at a heating rate of 10 °C min^{-1}. After 30 min reaction, the samples were cooled to room temperature in N_2. The original shiny surface of the Cu film became gray in color.

Characterization

Cu_3Si nanowires were characterized using scanning electron microscopy (SEM) and transmission electron microscopy (TEM). For HRSEM imaging, images were obtained using a HITACHI-S4700 field-emission SEM and a JSM-7000F (JEOL) thermal-type field-emission SEM, operated at an accelerating voltage of 5–15 kV with working distances ranging between 10 and 20 mm. For HRTEM imaging, the TEM samples were prepared by either drop-casting nanowires from toluene dilute dispersions onto 200-mesh lacey carbon-coated copper (gold) grids (Electron Microscope Sciences) or dry transferring by scratching the grids on the surface of the nanowire-deposited substrates. Images were acquired using an accelerating voltage of 200 kV on a Philips Technai G2 and JEOL JEM-2100F and an accelerating voltage of 300 kV on a JEOL JEM-3000F with all equipped with an Oxford INCA EDS spectrometer and a high angle annular dark field detector (HAADF). EDS measurements were taken of wires suspended under vacuum to minimize background signal. X-ray diffraction (XRD) was performed with a Rigaku Ultima IV X-ray diffractometer using Cu Kα radiation ($\lambda = 1.54$ Å). Nanowires were deposited onto quartz or glass substrates at a scan rate of 1° min^{-1}, and Cu_3Si films were characterized without further treatment. The chemical bonds of shell components were analyzed by a high resolution X-ray Photoelectron Spectrometer (XPS, PHI Quantera SXM/Auger: AES 650). Samples were prepared by depositing nanowires onto a titanium substrate (0.25 cm^2). Attenuated Total Reflectance Fourier transform Infrared spectroscopy (ATR-FTIR) was performed using a Perkin Elmer RXI FTIR System. Background scans were first taken of a clean ATR stage. Reflectance measurements were performed with a Hitachi U-4100 spectrophotometer employing deuterium and tungsten lamps, and equipped with a 60 mm integrating sphere. Reflectance spectra were referenced to Cu films (500 nm) or the Cu substrate. The field emission properties of Cu_3Si nanowires were obtained in a Keithly model 237 system with the geometry of the parallel plates with a spacing of 200 μm at a pressure of 3×10^{-6} torr. The contact area was 0.09 cm^2. The emission current was recorded with the applied voltage increasing at steps of 20 V at a time.

Results and discussion

Cu_3Si nanowires were synthesized by thermal decomposition of MPS in the presence of the Cu seed substrate, *i.e.*, Cu metal or Cu film-covered substrate, at 420 to 475 °C and 10.3 MPa in supercritical benzene. MPS was decomposed *via* disproportionation reactions to provide sufficient Si atoms to react with Cu substrates. Fig. 1 shows the synthesis result. It presents the XRD pattern of Cu_3Si nanowires with the diffraction peaks at $2\theta = 36.6$, 44.6, 45.0, 49.6, and 78.0°, corresponding to η-Cu_3Si (JCPDS 51-0916).[26] No peaks corresponding to Si were detected. Fig. 2a shows a top-view image of low magnification revealing the high density and high aspect ratio of Cu_3Si nanowires. A cross-sectional SEM image of the sample (Fig. 2b) reveals that the Cu_3Si nanowire arrays are randomly aligned with respect to the substrate surface. Closer imaging of Cu_3Si nanowires shows the nanowire diameters ranging from 50 to 150 nm with lengths typically over 10 μm (Fig. 2c).

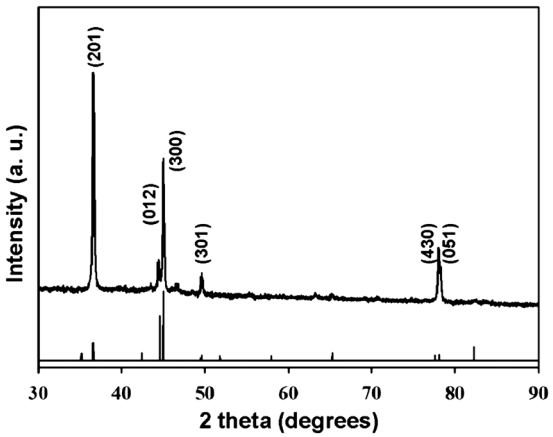

Fig. 1 XRD pattern of solution-grown Cu_3Si nanowires. Reference pattern: JCPDS 51-0916.

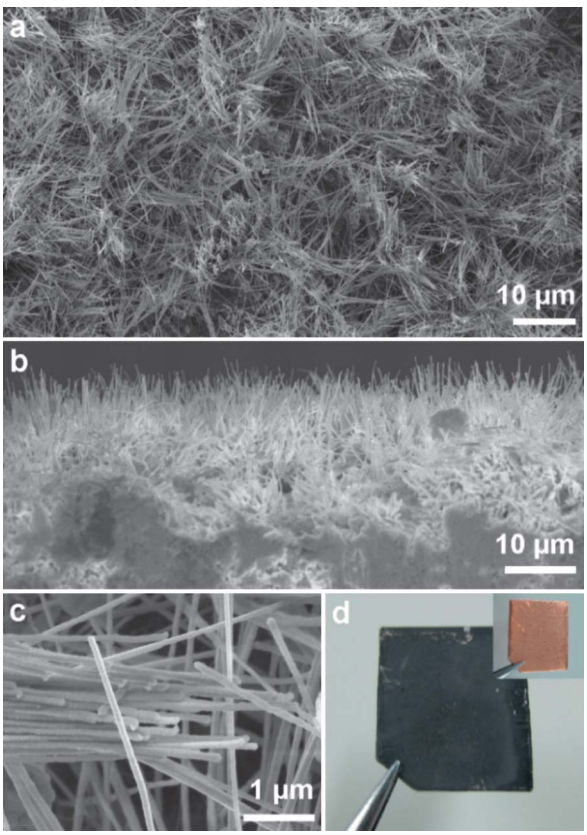

Fig. 2 (a) Top-view and (b and c) side-view SEM images of Cu_3Si nanowires grown on a Cu substrate. (d) Photographs of the Cu substrate before (inset) and after a reaction.

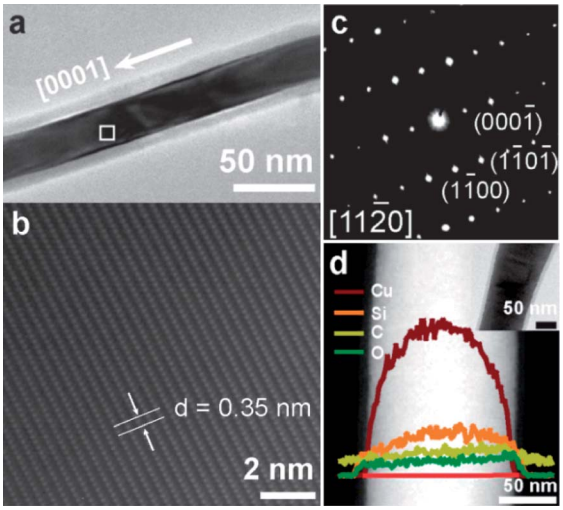

Fig. 3 (a) TEM image of a Cu_3Si nanowire. (b) HRTEM image of the area marked with a square in panel a, showing the single crystalline structure. (c) The corresponding selected area electron diffraction pattern of the wire. (d) EDS line-scan profile of Cu, Si, O, and C acquired across the nanowire.

A significant color change of the Cu substrate before and after nanowire reactions was observed. Both sides of the copper substrate were homogeneously covered with Cu_3Si nanowire films which appeared black (Fig. 2d), whereas the Cu substrate appeared brownish in color. The Cu_3Si nanowire synthesis can also be carried out using hexane as the solvent (Fig. S1†). TEM images of the Cu_3Si nanowires are displayed in Fig. 3 and S2.†

The nanowires were coated with an amorphous layer with a smooth surface and with a thickness of 50 nm (Fig. 3a). Fig. 3b and c show the HRTEM image and the SAED pattern taken along the [11–20] zone axis of a nanowire. The growth direction of the nanowire is determined to be [0001].[27] From the FFT pattern, satellite spots are observed because of the existence of the long-period anti-phase domain (LPAPD). Such patterns have been reported previously from epitaxial Cu_3Si nanostructures and thin films grown on silicon.[27,28] The amorphous layer coated on Cu_3Si nanowires has a shell thickness ranging from 10 to 15 nm. To investigate the elemental composition of the shell, a detailed chemical analysis was carried out using energy dispersive X-ray spectroscopy (EDS). The EDS line-scan profile of Cu, Si, O, and C acquired across the Cu_3Si nanowire is shown in Fig. 3d. The Cu and Si signals were strongest when the beam was positioned within the crystalline core of the nanowire. When the beam was positioned in the shell, the Si signal decreased in intensity and small oxygen and carbon signals were detected in the shell with no detectable Cu signal, confirming that the shell is composed of Si, C, and O.

In order to determine the shell composition, X-ray photoelectron spectroscopy (XPS) and Fourier transform Infrared spectroscopy (FTIR) were used. Fig. 4 shows the Si 2p, C 1s, and O 1s XPS spectra of the Cu_3Si nanowire. There is an intense peak in the Si 2p binding region at ~102.7 eV, C1s at ~284.1 eV, and O1s at ~532.0 eV. The curve-fitted Si 2p core levels at 101.3, 102.6, and 103.5 eV, C 1s core levels at 283.4, 284.1, and 285.2 eV,

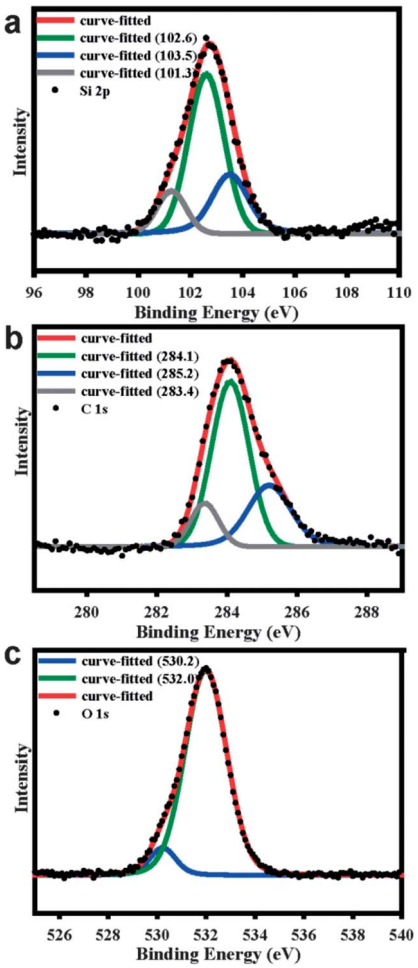

Fig. 4 XPS spectra of Cu_3Si nanowires: (a) Si 2p, (b) C 1s, and (c) O 1s.

and O 1s core levels at 530.2 and 532 eV indicated that the shell was composed of polysiloxanes.[29,30] Furthermore, the FTIR spectrum also showed the presence of polysiloxanes. The peak around 1100–1000 cm^{-1} is due to the X-sensitive band from the Si–Ph bond or the asymmetric Si–O–Si stretching (Fig. S3†). The peaks around 2400 cm^{-1} and 2900 cm^{-1} are due to the alkyl group.[31] From the XPS and FTIR results, the shell of Cu_3Si nanowires is composed of polysiloxane, which results from the slow oxidation of polysilanes to polysiloxanes on exposure to oxygen. The polysiloxane shell from side-wall deposition of MPS was also found in Au-seeded Si nanowires obtained by supercritical fluid synthesis using MPS as the precursor.[32]

We propose the growth mechanism for the solution-phase synthesis of Cu_3Si nanowires by following the Si–Cu reactions between Si's influx and Cu's out-diffusion from the Cu layer. When Si atoms are deposited onto the surface of a Cu substrate, the lattice Cu–Cu bonds are broken to cause out-diffusion of Cu from the Cu substrate. Due to the high diffusivity and high solubility of Cu with respect to Si ($D = 2.0 \times 10^{-5}$ cm^2 s^{-1} at 500 °C),[33] a copper silicide layer readily forms and serves as an intermediate layer for further diffusion of Si and Cu. Various silicide phases may form sequentially starting from Si-rich to Cu-rich phases. The phase formulation sequence in the reaction between

MPS and the copper substrate may be different because Cu's diffusion rate and Si's generation rate are dependent on reaction temperature and MPS concentration. After Si atoms are continuously deposited onto the surface, nucleation of Cu_3Si nanoparticles occurs, as shown in Fig. 5a. The nucleation of copper silicide nanoparticles means that supply of the underlying copper is fast enough to diffuse into the overlying silicide associated with diffusion-limited reactions. These nanoparticles serve as seeds for further anisotropic growth outwards from the surface (Fig. 5b). Continuous out-diffusion of Cu proceeds through the pre-formed copper silicide layer. The rate of Cu's outflux and Si's influx reaches optimal balance to promote arrays of Cu_3Si nanowires propagating outwards from the substrate (Fig. 5c). The cross-section image at the connection between the Cu_3Si nanowire and the copper substrate shows cracking and depletion of the Cu substrate (Fig. 5c and d), demonstrating that Cu is a fast diffuser relative to Si. Recently, Holmberg *et al.* also found that Cu_3Si can form violently when the Cu grid comes into contact with Si nanowires due to the extremely fast rate of Cu diffusion to the Si layer.[34] The overall growth rate was around 5 μm min^{-1}, which is comparable to the rates measured in vapor-phase grown copper silicide and nickel silicide nanowires.[7,10,11,15] As shown in Fig. 5e, there appear tips at the top ends of each silicide nanowire. TEM images of these tips show that the diameters of the tips are generally larger than the nanowires themselves, but with distinct morphologies. The atomic ratios of the elements of the tip and the wire as detected from EDS are almost the same (~76 at% Cu and ~24 at% Si), showing compositional homogeneity of the tip and the nanowire body (Fig. 5f–h). The HRTEM images and FFT patterns of the tip and the nanowire are also identical (Fig. 6). These findings provide strong evidence that the overall nanowire growth follows the self-catalyzed reactions driven by diffusion-limited growth without employing any other catalysts, with the growth mechanism similar to that of nickel silicide nanowires synthesized by chemical vapor transport of Si on Ni foil.[10,11]

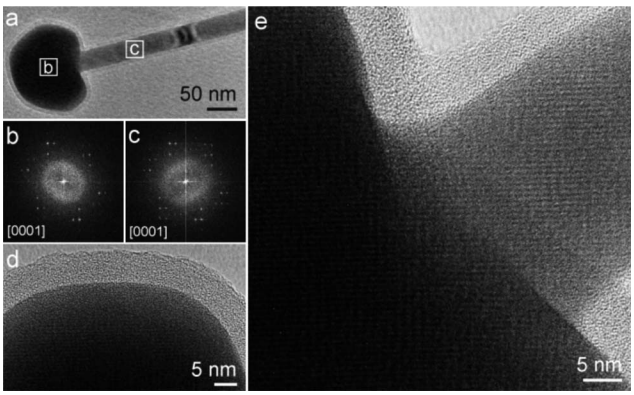

Fig. 6 TEM images of a Cu_3Si nanowire with a tip. (b and c) FFT patterns taken from the tip and the nanowire body, respectively. HRTEM images of (d) the tip and (e) the interface.

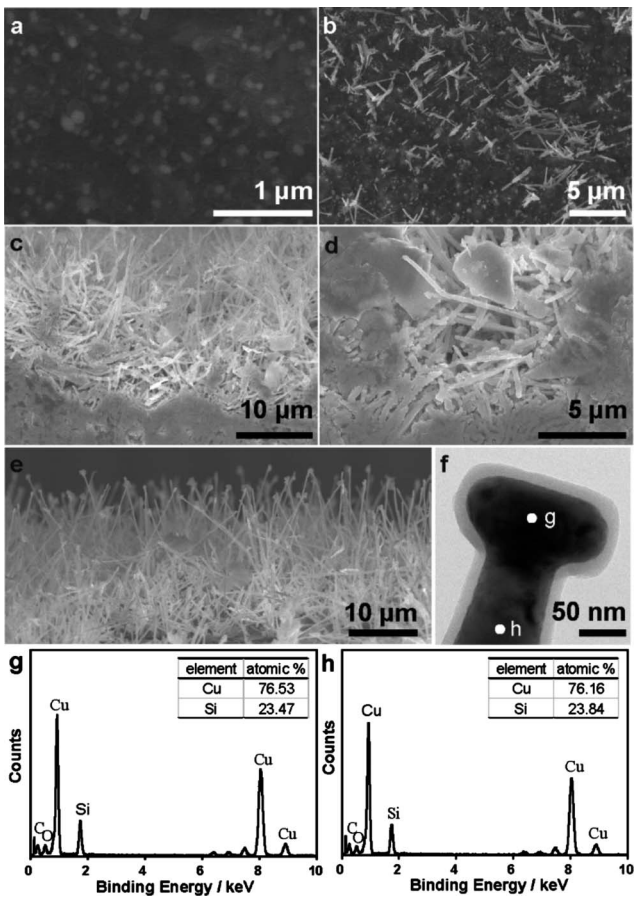

Fig. 5 (a–c) SEM images of the reaction products at different stages: (a) beginning, (b) 1 min and (c) 5 min. (d) Side-view SEM image of the interface between Cu_3Si nanowires and a Cu substrate. (e) Side-view SEM image showing tips at the top ends of Cu_3Si nanowires. (f) TEM image of a Cu_3Si nanowire with a tip end. (g and h) EDS taken at the tip and the nanowire body, respectively.

Fig. 7 shows the field emission performance of self-aligned Cu_3Si nanowires with the current density as a function of the macroscopic electric field. The turn-on voltage (defined as the electric field that produces a current density of 10 μA cm^{-2}) is estimated to be 1.16 V μm^{-1} (Fig. S4†), much smaller than that reported in previous studies on metal silicide nanowires such as tantalum silicide, nickel silicide and titanium silicide nanowires, with the turn-on voltages (for a current density of 10 μA cm^{-2}) in the range of 3–4 V μm^{-1}.[35–38] Strong mechanical

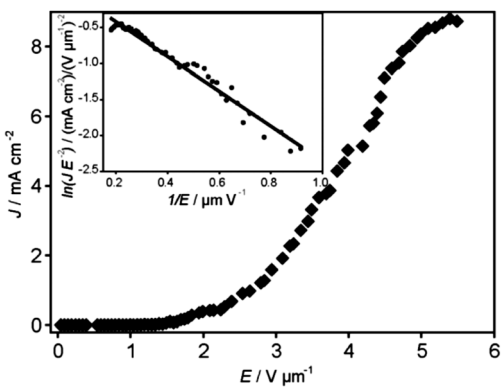

Fig. 7 Electron field emission profile of Cu_3Si nanowires grown on a Cu substrate. The inset shows the corresponding F–N plot. J (mA cm^{-2}) is the emission current density and E (V μm^{-1}) is the applied electric field.

adhesion and good electrical contact between nanowires and the Cu substrate allow efficient electron injection and transmission through nanowires so as to obtain very low turn-on voltage. The emission current density of 8 mA cm^{-2} was obtained at 4.9 V μm^{-1}. The inset in Fig. 7 is a plot of $\ln(JE^{-2})$ *versus* $1/E$, yielding a straight line and is in good agreement with the Fowler–Nordheim (F–N) equation given by the following:

$$J = (A\beta^2E^2/\Phi)\exp(-B\Phi^{3/2}/\beta E)$$

A and B are constants, corresponding to 1.56×10^{-10} (A eV V^{-2}) and 6.83×10^3 (V $eV^{-3/2}$ μm^{-1}), respectively. J is the current density, β is the field enhancement factor, and Φ is the work function of emitter materials. Assuming Φ to be equal to 4.7 eV for Cu_3Si, β can be calculated from the slope of the FN plot and is calculated to be 1499.

To realize many practical uses, it is necessary to grow nanowires on a variety of substrates or grow them at specific locations on the substrate.

However, conventional gas-phase silicide nanowire growth requires relatively high growth temperature, thus greatly restricting the integration of nanowires on polymer or glass based devices. In our study, relatively low reaction temperatures enable the direct synthesis of Cu_3Si nanowires on a wide range of substrates. Fig. 8 shows the representative optical image of Cu_3Si nanowires grown on glass (Fig. 8a), a flexible plastic polyimide (PI) substrate (Fig. 8b), and large area (6.5 cm × 5 cm) flexible copper foil (Fig. 8c). All samples present the same black appearance, showing that Cu_3Si nanowire arrays were obtained. As shown in Fig. 8b, nanowire growth on a PI substrate can be subjected to extremely large deformations. The nanowires were still firmly anchored on the PI after bending. Furthermore, Cu_3Si nanowires can be grown at predetermined sites on arbitrary substrates by patterning the Cu film in specific regions prior to the growth. Cu_3Si nanowires were grown on a PI substrate patterned with a copper thin film by a standard microfabrication lift-off process. SEM images show the nanowires formed in the copper patterned regions (Fig. 8d and S5†). The self-supported, patternable Cu_3Si nanowire arrays on polymer substrates represent a novel architecture for foldable or flexible devices.

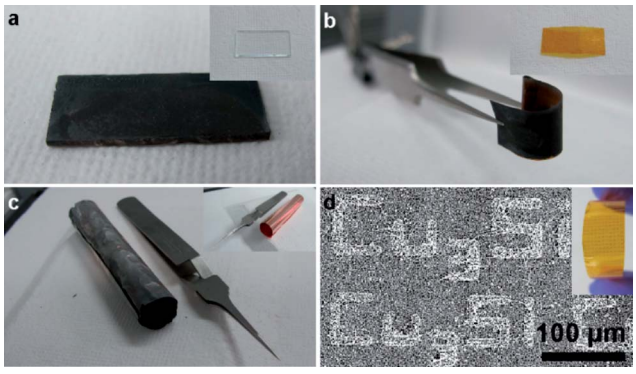

Fig. 8 Digital photographs and SEM image of Cu_3Si nanowires grown on (a) Cu film-coated glass, (b) plastic PI substrate, (c) 6.5 cm × 5 cm flexible copper foil, and (d) PI substrate patterned with Cu patterns.

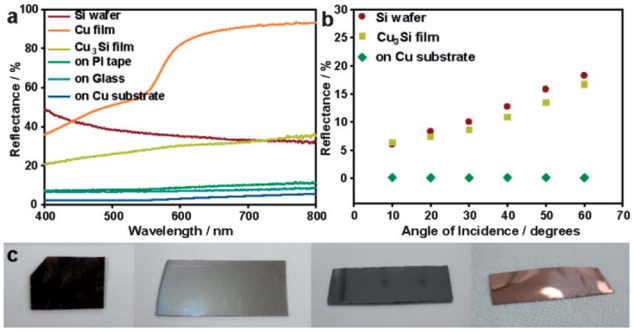

Fig. 9 (a) Total reflectance spectra of a Cu film, Si wafer, Cu_3Si film, and Cu_3Si nanowire grown on different substrates. (b) The angle-dependent reflectance measurements at 780 nm for a Si wafer, Cu_3Si film, and Cu_3Si nanowire grown on a Cu substrate. (c) Left to right: photographs of Cu_3Si nanowire grown on a Cu substrate, Cu_3Si film, Si wafer, and Cu film.

Black Cu_3Si nanowire films on each substrate demonstrate efficient antireflection properties as dielectric antireflection coatings for the enhancement of light trapping in applications such as photovoltaic devices. Fig. 9a depicts the quantified total reflectance for Cu_3Si nanowires grown on different substrates at normal incidence *versus* wavelength. One can clearly observe the total reflectance of Cu_3Si nanowires grown on a Cu substrate ranging from 2 to 5% over a wide spectral bandwidth from the wavelength of 400 to 800 nm, giving highly efficient antireflection properties. These values are significantly smaller than those of the planar Si wafer (30 to 50%) and the Cu_3Si film (20 to 35%). The antireflective properties originated from the randomly oriented arrays of the nanowires. Furthermore, Cu_3Si nanowires grown on glass and flexible plastic also exhibited excellent reflectance less than 7% in the wavelength range from 400 to 800 nm. The remarkable low reflectance may be attributed to random alignment and dense distribution of Cu_3Si nanowires that can effectively enhance the anti-reflection property by trapping light, leading to broadband suppression in reflection.

In general, dense arrays of nanowires with a high aspect ratio were found to possess very good absorption characteristics towards sunlight since incident light is scattered between the nanowires.[7] Angle dependent reflectance measurements were also performed on Cu_3Si nanowires. Fig. 9b shows the specular reflectance spectra of the Cu_3Si nanowires grown on a Cu substrate, Cu_3Si film, and Si wafer with the incident angle varied from 10 to 60 degrees with a wavelength of 780 nm. This angle dependent measurements show that Cu_3Si nanowires exhibit extremely minimal reflectance (~0.1%), even at high incident angles. Fig. 9c shows the photographs of the Cu_3Si nanowires grown on a Cu substrate, a Cu_3Si thin film grown on a Si wafer, a Si wafer, and a Cu film, from left to right, to compare their optical appearance.

Conclusions

Dense, self-aligned single-crystal Cu_3Si nanowires were synthesized by solution-phase, diffusion-based silicidation reactions at relatively low temperatures from 420 to 475 °C.

Cu_3Si nanowire arrays give strong optical absorption as antireflective coatings for photovoltaic devices, high current outputs, possess excellent field emission properties, and can be directly grown on a wide range of substrates. The solution-phase silicidation may be applicable to grow other silicide nanowires. This study demonstrates that diffusion-based silicide reactions could be applicable in solution phase to promote silicide nanowire growth with a growth rate comparable to that of the gas-phase growth, thus expanding the availability of nanomaterial chemistry in solution-phase synthesis. Moreover, associated promising properties obtained from the solution-grown Cu_3Si nanowires demonstrate the promise of solution-phase reactions to fabricate metal silicide-based devices.

Acknowledgements

The authors acknowledge the financial support by the National Science Council of Taiwan (NSC NSC 100-2628-E-007-029-MY2, 102-2221-E-007-023-MY3, NSC 102-2221-E-007-090-MY2, and NSC 101-2623-E-007-013-IT), the Ministry of Economic Affairs, Taiwan (101-EC-17-A-09-S1-198), National Tsing Hua University (102N2051E1, 102N2061E1), and the HRTEM (JEOL JEM-2100F) assistance from Tamkang University College of Science and the assistance from Center for Energy and Environmental Research, National Tsing-Hua University.

Notes and references

1 S. L. Zhang and U. Smith, *J. Vac. Sci. Technol., A*, 2004, **22**, 1361–1370.
2 J. P. Gambino and E. G. Colgan, *Mater. Chem. Phys.*, 1998, **52**, 99–146.
3 A. L. Schmitt, J. M. Higgins, J. R. Szczech and S. Jin, *J. Mater. Chem.*, 2010, **20**, 223–235.
4 C. I. Tsai, P. H. Yeh, C. Y. Wang, H. W. Wu, U. S. Chen, M. Y. Lu, W. W. Wu, L. J. Chen and Z. L. Wang, *Cryst. Growth Des.*, 2009, **9**, 4514–4518.
5 L. Dong, J. Bush, V. Chirayos, R. Solanki, J. Jiao, Y. Ono, J. F. Conley and B. D. Ulrich, *Nano Lett.*, 2005, **5**, 2112–2115.
6 J. Kim, Y. H. Shin, J. H. Yun, C. S. Han, M. S. Hyun and W. A. Anderson, *Nanotechnology*, 2008, **19**, 485713.
7 N. P. Dasgupta, S. Xu, H. J. Jung, A. Iancu, R. Fasching, R. Sinclair and F. B. Prinz, *Adv. Funct. Mater.*, 2012, **22**, 3650–3657.
8 J. Kim, D. H. Shin, E. S. Lee, C. S. Han and Y. C. Park, *Appl. Phys. Lett.*, 2007, **90**, 253103.
9 C. Y. Lee, M. P. Lu, K. F. Liao, W. W. Wu and L. J. Chen, *Appl. Phys. Lett.*, 2008, **93**, 113109.
10 C. J. Kim, K. Kang, Y. S. Woo, K. G. Ryu, H. Moon, J. M. Kim, D. S. Zang and M. H. Jo, *Adv. Mater.*, 2007, **19**, 3637–3642.
11 K. Kang, S.-K. Kim, C.-J. Kim and M.-H. Jo, *Nano Lett.*, 2008, **8**, 431–436.
12 K. Yamamoto, H. Kohno, S. Takeda and S. Ichikawa, *Appl. Phys. Lett.*, 2006, **89**, 083107.
13 B. Liu, Y. Wang, S. Dilts, T. S. Mayer and S. E. Mohney, *Nano Lett.*, 2007, **7**, 818–824.
14 C. H. Chiu, C. W. Huang, J. Y. Chen, Y. T. Huang, J. C. Hu, L. T. Chen, C. L. Hsin and W. W. Wu, *Nanoscale*, 2013, **5**, 5086–5092.
15 H. Geaney, C. Dickinson, C. O'Dwyer, E. Mullane, A. Singh and K. M. Ryan, *Chem. Mater.*, 2012, **24**, 4319–4325.
16 L. Ouyang, E. S. Thrall, M. M. Deshmukh and H. Park, *Adv. Mater.*, 2006, **18**, 1437–1440.
17 K. S. K. Varadwaj, K. Seo, J. In, P. Mohanty, J. Park and B. Kim, *J. Am. Chem. Soc.*, 2007, **129**, 8594–8599.
18 A. L. Schmitt, M. J. Bierman, D. Schmeisser, F. J. Himpsel and S. Jin, *Nano Lett.*, 2006, **6**, 1617–1621.
19 A. L. Schmitt, L. Zhu, D. Schmeißer, F. J. Himpsel and S. Jin, *J. Phys. Chem. B*, 2006, **110**, 18142–18146.
20 A. L. Schmitt, J. M. Higgins and S. Jin, *Nano Lett.*, 2008, **8**, 810–815.
21 B. A. Korgel, *AICHE J.*, 2009, **55**, 842–848.
22 K. M. Ryan, D. Erts, H. Olin, M. A. Morris and J. D. Holmes, *J. Am. Chem. Soc.*, 2003, **125**, 6284–6288.
23 H. Y. Tuan, D. C. Lee and B. A. Korgel, *Angew. Chem., Int. Ed.*, 2006, **45**, 5184–5187.
24 F. W. Yuan, H. J. Yang and H. Y. Tuan, *J. Mater. Chem.*, 2011, **21**, 13793–13800.
25 C. A. Barrett, R. D. Gunning, T. Hantschel, K. Arstila, C. O'Sullivan, H. Geaney and K. M. Ryan, *J. Mater. Chem.*, 2010, **20**, 135–144.
26 Z. Zhang, L. M. Wong, H. G. Ong, X. J. Wang, J. L. Wang, S. J. Wang, H. Chen and T. Wu, *Nano Lett.*, 2008, **8**, 3205–3210.
27 S. J. Jung, T. Lutz, A. P. Bell, E. K. McCarthy and J. J. Boland, *Cryst. Growth Des.*, 2012, **12**, 3076–3081.
28 C. Y. Wen and F. Spaepen, *Philos. Mag.*, 2007, **87**, 5581–5599.
29 L. A. O'Hare, B. Parbhoo and S. R. Leadley, *Surf. Interface Anal.*, 2004, **36**, 1427–1434.
30 S. Roualdes, R. Berjoan and J. Durand, *Sep. Purif. Technol.*, 2001, **25**, 391–397.
31 S. Jolly, J. Saussey and J. Lavalley, *Catal. Lett.*, 1994, **24**, 141–146.
32 H.-Y. Tuan and B. A. Korgel, *Chem. Mater.*, 2008, **20**, 1239–1241.
33 T. Heiser and A. Mesli, *Appl. Phys. A: Solids Surf.*, 1993, **57**, 325–328.
34 V. C. Holmberg, K. A. Collier and B. A. Korgel, *Nano Lett.*, 2011, **11**, 3803–3808.
35 Z. Liu, H. Zhang, L. Wang and D. Yang, *Nanotechnology*, 2008, **19**, 375602.
36 B. Xiang, Q. Wang, Z. Wang, X. Zhang, L. Liu, J. Xu and D. Yu, *Appl. Phys. Lett.*, 2005, **86**, 243103.
37 H. K. Lin, Y. F. Tzeng, C. H. Wang, N. H. Tai, I. N. Lin, C. Y. Lee and H. T. Chiu, *Chem. Mater.*, 2008, **20**, 2429–2431.
38 Y. Chueh, L. Chou, S. Cheng, L. Chen, C. Tsai, C. Hsu and S. Kung, *Appl. Phys. Lett.*, 2005, **87**, 223113.